 doi:10.20944/preprints202101.0422.v1

On the Role of Grain Boundaries During Sintering

Torsten E.M. Staab[1,2], Ricardo Helm[1,2], and Andreas Diegeler[2]

[1]*University Würzburg, Dep. of Chemistry – LCTM, Röntgenring 11, D-97070 Würzburg, Germany*

[2]*Fraunhofer Institute for Silicate Research, Neunerplatz 2, D-97082 Würzburg, Germany*

Corresponding author e-mail: torstenstab@uni-wuerzburg.de

We present new results in positron annihilation lifetime spectroscopy (PALS), thermo-optical dilatometry and microscopy, which are indicating a strong correlation between grain-boundaries and mass transport during the sintering process of carbonyl iron powder. In this particular system we were able to show that the change in particle shape and size with increasing temperature yields an anisotropy in shrinkage, which manifests itself in a higher shrinkage perpendicular to the compaction axis. In the intermediate stage of sintering, where the major mass transport occurs, the average distance between two grain boundaries could be determined to (3,73 ± 0,18) µm at T = 744°C. This is in good agreement with previous calculations of positron pathways in defect free particles. Furthermore, due to sintering temperatures far above the annealing temperature of dislocations in iron, the existence of dislocations in the bulk of the particles is very unlikely. These claims are reflected by the collected positron data, which exhibit a clear grain boundary signal of ~ 250ps while no vacancy or dislocation signal (typically ~ 160 ps) is evident in the intermediate stage of sintering.

Keywords:
Grain Boundaries, Sintering

I. INTRODUCTION

Sintering PM parts without pressure is the most cost-effective way [1]. Therefore, it is widely used. However, uniaxial compaction may result in regions of different density. Hence, we do employ an optical dilatometer possessing an optical window of 50mm in diameter, e.g. detecting changes in their width, height or surface area [2,3]. So, as shown previously [4,5], one can monitor changes in the size of large samples of arbitrary shape at different regions during the same run [4,5]. A conventional dilatometer does offer a better precision, but not this possibility. Additionally, very delicate samples or ones having an irregular shape can be monitored in an optical dilatometer as used in this study.
There are additional applications of the TOM-AC: It is possibility to optimize the time-temperature cycle for powder metallurgical (PM) products by measuring the weight-loss during de-binding, the shrinkage during sintering or even exerting a force on the sample. Since the production of PM parts is an energy intensive process in industry, it can be optimized so that the inevitable heat treatments can be performed as effective as possible.
Positron annihilation spectroscopy is able to detect lattice defects like vacancies, dislocations and grain boundaries. Since these lattice defects are assumed to influence the solid-state sintering to a large extent, we have applied the method of positron annihilation lifetime spectroscopy here.
This article is outlined as follows. First we give a short introduction to the principle of thermo-optical measurements. Then we present details of the investigated samples. Finally, we discuss how the microstructure influences the shrinkage.

II. EXPERIMENTAL: OPTICAL DILATOMETRY AND SAMPLES

TOM-AC – our optical dilatometer – consists of a cylindrical vacuum vessel containing a metallic Mo-heater, making measurements under reducing or inert gas conditions possible. We employed this heater under reducing or inert gas atmosphere for all experiments.
The vacuum vessel has two cylindrical openings on the optical axis, which are equipped with optical flanges (quartz glass) located at 180°. This allows to view the sample in backlight.
Employing temperatures below 1300°C (low temperature range used here) the sample is illuminated from the left, while the CMOS-camera detects the sample's silhouette inside the furnace in backlight from the right (see figure 1). The used improved version of TOM-AC has a blue light source equipped with a diode-array illuminating an Ulbricht sphere to make the distribution of light smooth. The short wavelength (blue) improves the accuracy compared to white light. At temperatures higher than 1300°C (high temperature range – not used here) the sample is self-luminous so that the diode-array can be switched off. Figure 1 shows the experimental set-up.

Preprints (www.preprints.org) | NOT PEER-REVIEWED | Posted: 21 January 2021 doi:10.20944/preprints202101.0422.v1

Since the glass windows do not insulate as well as the furnace's insulation, most of the infrared radiation must be reflected back into the furnace – done here by transparent gold mirrors mounted outside the optical flanges, resulting in a homogeneity of about 1K/cm inside the furnace at the sample's position.

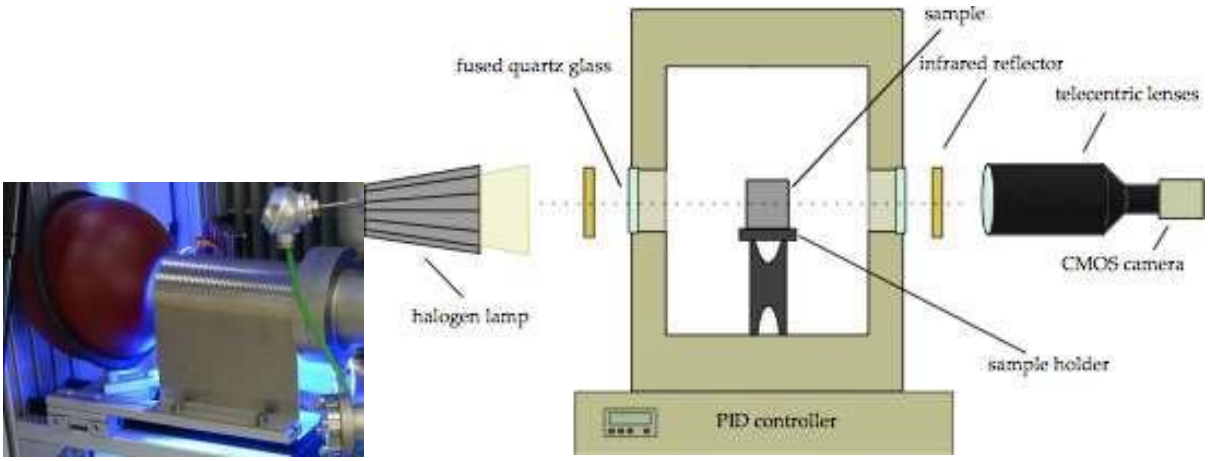

Figure 1: Schematic view of the thermo-optical measurement device TOM-AC at the Fraunhofer ISC (right) and diode light source with Ulbricht sphere (left): Samples are placed inside a furnace enclosed by a vacuum vessel. This allows for a vacuum of better than 10^{-5}mbar. The sample is illuminated from the left while the CMOS-camera placed to the right detects its shape. Temperature control is realised either by a thermocouple or a pyrometer.

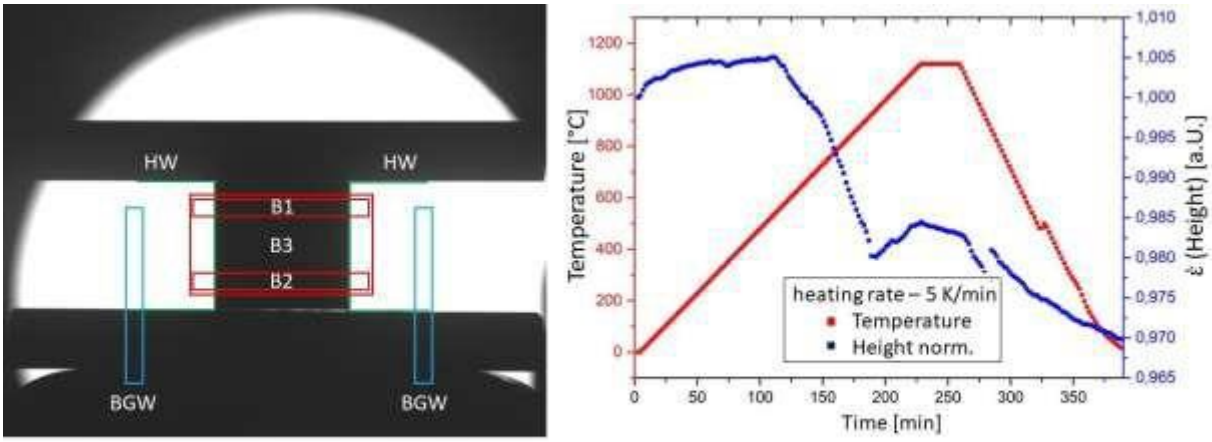

a) b)

Figure 2: Schematic silhouette of the cylindrical carbonyl iron sample inside the furnace of TOM-AC (a) and the heating ramp / shrinkage in height (b): The bright circular part in (a) shows the size of the optical window (diameter: 50mm) while the sample appears dark in the backlight. The sample is placed between two alumina plates for a more precise detection of the height. The contour detection algorithm scans the shape (green) while the chosen background windows (BGW - blue) are shown to both sides of the sample. Shown here are three widths (in red – fig. 4) used to measure the shrinkage and, additionally, the shrinkage curve for the height (HW) (b).

By averaging over 150 frames, the software corrects imaging errors like noise and thermal flickering [2,3]. Simultaneously the exposure time is adapted to the brightness to enhance the contrast by keeping it within the dynamic range of the CMOS-sensor. The telecentric optic ensures that the imaged sample size is independent of the exact sample position.
Temperature control is realized by a PID-controller. It senses the temperature either by a Pt-Rh-thermocouple (type B) inside the furnace or by a pyrometer pointing to the sample.

All CMOS-camera pictures are analysed in real-time by employing a Monte-Carlo algorithm [2] to determine the sample's contour with the smallest possible systematic error. The windows for recording the dimensional changes are shown in figure 2 and 4. They are chosen by the user. Once the width

Preprints (www.preprints.org) | NOT PEER-REVIEWED | Posted: 21 January 2021 doi:10.20944/preprints202101.0422.v1

and height windows have been positioned, they are kept at the same sample position during one run by the use of background windows. This way the sample region actually recorded always remains the same, independent of the thermal expansion of both sample and sample holder. The software is recording the relative change of the sample's width and/or height $\varepsilon = L/L_0$ and also stores the pictures taken.

All sample have been prepared from the same carbonyl iron powder with a typical purity of 2N. The powder has mainly a spherical geometry and a powder particle size of <10µm. The nearly spherical form makes carbonyl iron to a well-suited model system.
The green samples have been prepared by uniaxial compaction. For the shrinkage curves recorded in the TOM-AC, cylindrical samples of 11mm in height and diameter have been prepared. For the investigations by positron annihilation spectroscopy we prepared disks of the same diameter with a thickness of about 1mm. We performed the heat treatment by interrupted sintering in the following way: the samples where heated with a certain heating rate inside a vacuum tight furnace under flowing gas (mixture of Ar and 6%H). When the target temperature was reached, the furnace was opened and the samples were rapidly cooled by cold nitrogen gas. Uniaxial compaction typically leads to more compacted areas close to the punch, i.e. at the upper and lower parts of the cylindrical samples.
Positron annihilation lifetime spectroscopy (PALS) has been established in the past decades as a powerful tool for the detection of lattice defects in crystalline materials like semiconductors and metals. It measures the lifetime of a positron in a sample: e.g. τ_{bulk} =106ps in the ideal iron bcc-lattice [6,7]. This method responds very sensitive to defects in the crystalline lattice. In metals typical lattice defects detected by positrons are mostly related to (mono-) vacancies, dislocations, small vacancy clusters, but also precipitates, interfaces, and inner surfaces (pores) [8,9,10]. All defects lead to characteristically longer positron lifetimes (compared to the bulk) due to their locally lower electron densities [10]: e.g. τ =175ps for vacancies or τ =165ps for dislocations [6] both in iron or 500-600ps for metallic surfaces in general. In general, an increasing defect density, i.e. higher dislocation densities or smaller grain/particle sizes, lead to an increased average positron lifetime. For more details we refer to [9,11,10].

III. MICROSTRUCTURE: CARBONYL IRON

The microstructure after compaction (see fig. 3) shows an as-pressed sample prepared by standard metallography. By the Feret method we have recorded the average powder particle size leading to a value of (1,95 ± 0,08) µm at before sintering and (3,73 ± 0,18) µm for sintering up to T = 744°C.

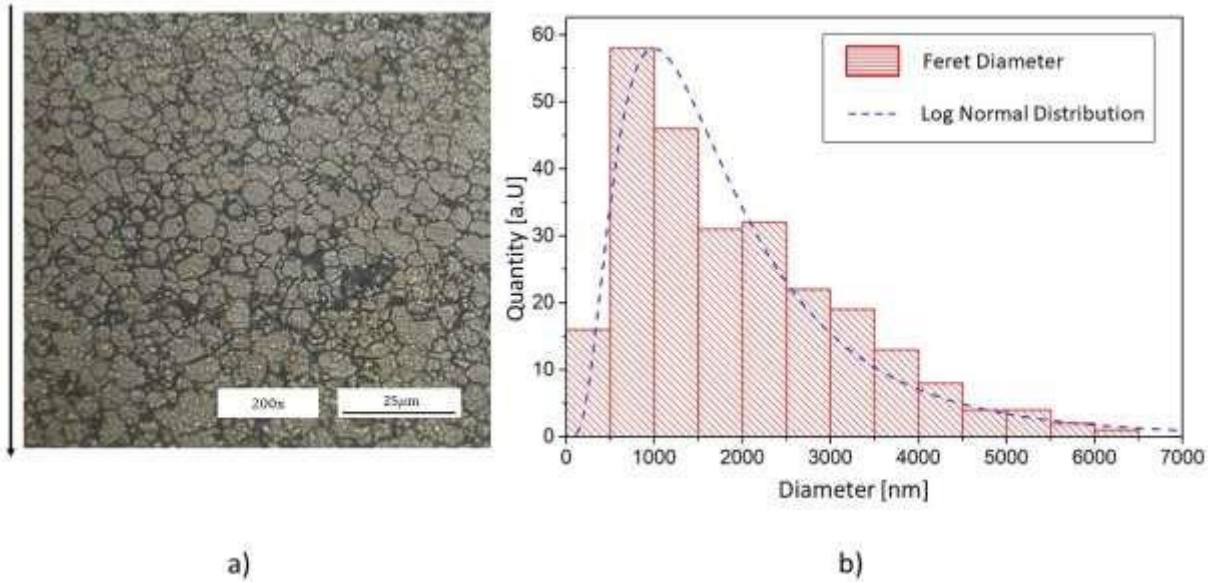

Figure 3: Metallographically prepared sample (left - a): powder compact. The black arrow denotes the compaction direction. The particle size distribution determined by the Feret method is shown on the right (b).

Preprints (www.preprints.org) | NOT PEER-REVIEWED | Posted: 21 January 2021 doi:10.20944/preprints202101.0422.v1

IV. SHRINKAGE: CARBONYL IRON

Shrinkage and shrinkage rate are shown in figure 4 and 5, respectively. The shrinkage during sintering has been recorded by TOM-AC under Ar-atmosphere containing 6.5% hydrogen.
The onset of shrinkage is just below 600°C while the rate has its maximum at about 800°C, when the carbothermic reaction of removing the oxides is most active [12]. The reduction of the oxides – supported by the hydrogen-containing atmosphere – makes the shrinkage possible. This is manifested in the high shrinkage rate observed at 800°C.

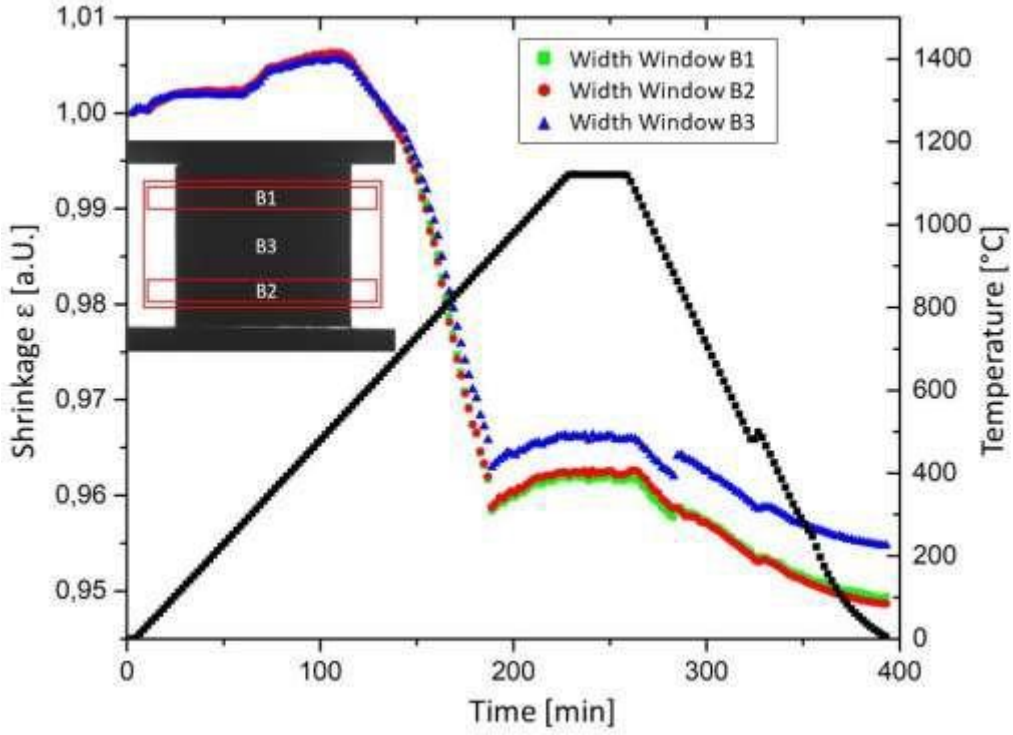

Figure 4: Carbonyl iron sample: heating ramp with 5 K/min up to 1120°C and shrinkage at three different positions (same measurement as in Fig. 2). Shown here are three widths (inset in red – B1, B2, B3) used to measure the shrinkage, e.g. upper and lower part of the sample as well as over the total width. The upper and lower part (B1 – red dots and B2 – green dots) show a nearly identical shrinkage, while the middle part obviously lags behind.

As can be seen from figure 4 the shrinkage in the middle part of the sample, which typically is not as much compacted as the upper and lower parts, lags behind during the heating up and cannot catch up during the isothermal phase. By using the optical dilatometer TOM-AC we have been able to record this within one measurement cycle so that all conditions are the same.
The reason for this behaviour is possibly the lower density in the middle part of the sample, which hinders the compaction. There are different theories explaining this: one employs the so-called “defect-activated sintering”, which assumes dislocations created by pressing the powder as the cause for enhanced diffusivity. According to this assumption the shrinkage should be largest parallel to the compaction direction. In fact, we observe the opposite (see fig. 4). So, one has to find a different explanation for this observation, where one assumption could be the deformation of the initially spherical powder particles to ellipsoids [13]. Another explanation could be the increased porosity in the in the outer areas of the sample, which have a higher density.

V. POSITRON ANNIHILATION

We have shown for several PM samples treated by interrupted sintering (see fig. 5) that above the recrystallization temperature of half the melting temperature in Kelvin, no lattice defects like vacancies and dislocations exist in significant amounts (see fig. 5 when the average positron lifetime drops).
During the intensive shrinkage, the grain growth leads to a further decreasing signal of the average positron lifetime, since less positrons are trapped to grain boundaries (see e.g. [8,9]). This is leading to the effect that, at the beginning of the isothermal phase, positrons start to reach the residual pores (see explanation in [11,10]).

Preprints (www.preprints.org) | NOT PEER-REVIEWED | Posted: 21 January 2021 doi:10.20944/preprints202101.0422.v1

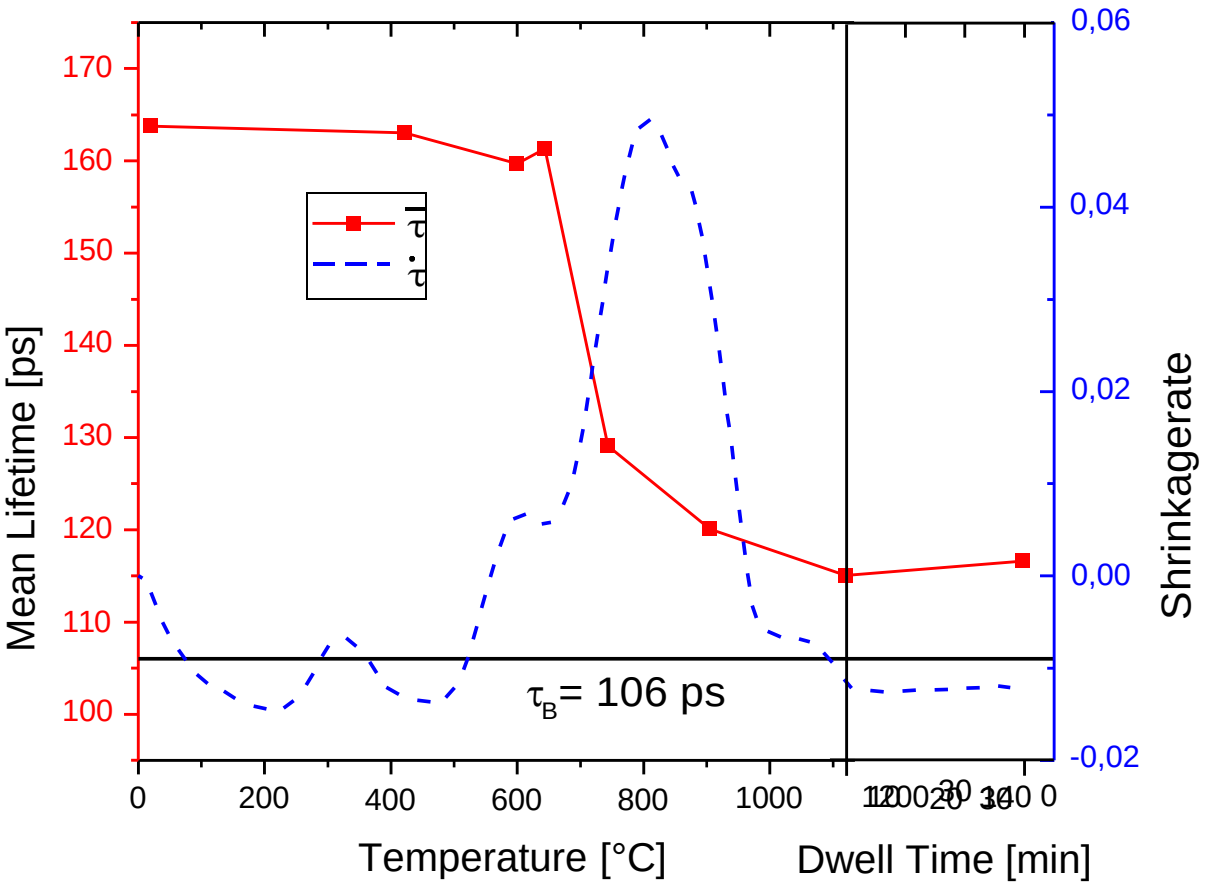

Figure 5: Carbonyl iron samples heated with 5 K/min up to 1120°C holding for 30min. The red squares show the average positron lifetime for the interrupted sintering, while the blue dashed line gives the shrinkage rate.

VI. CONCLUSIONS

We have shown the influence of lattice defects, determined by positron annihilation, on the sintering of carbonyl iron powder. This shows that during the heating up until a temperature of 632°C lattice defects (dislocations and grain boundaries) are existing, which lead to the increase average positron lifetime. For temperatures higher than 632°C the density of dislocations drops below the detection limit of about $3x10^8 cm^{-2}$. At these temperatures only grain boundaries exist as positron traps, when the shrinkage rate reaches its maximum. So, only volume or grain boundary diffusion are responsible for the observed shrinkage as claimed in [9,10].
For temperatures above 905°C, the shrinkage rapidly decreases while positron annihilation indicates merely the existence of pores as the only relevant microstructural features, being in accordance with the metallographic analysis. This means that the grain growth has been leading to grain sizes larger than 15-20µm. The final grain size determined after sintering amounts to (72.9±5.4)µm.

ACKNOWLEDGEMENTS

We would like to thank Prof. Dr.-Ing. Herbert Danninger and Assistant Prof. Dr.-Ing. Gierl-Mayer for providing us the carbonyl iron samples and the dilatometer data.

REFERENCES

01 R.M. German, *Powder Metallurgy Science*, 1st ed. Priceton, New Jersey, 1984
02 Friedrich G. Raether. *Current state of in situ measuring methods for the control of firing processes.* Journal of the American Ceramic Society, **92** (2009) 146–152

03 F. Raether, J. Meinhardt, P. Schulze Horn. *TOM – a versatile thermo-optical measuring system for the optimization of heat treatments.* CFI-Ceram. Forum Int. **84** (2007) E18

04 A. Diegeler and T. Staab, *Thermo-optical- measurement devices for powder metallurgical applications*, Proceedings of the Euro PM 2014, EPMA, European Powder Metallurgy Association (EPMA), Shrewsbury, United Kingdom

05 T.E.M. Staab and A. Diegeler, *Thermo-optical-measurement device for PM products under atmospheric controll*, Euro PM2015 Reims – Congress Proceedings, European Powder Metallurgy Association (EPMA), Shrewsbury, United Kingdom

06 Y.K. Park et al. *Dislocation studies on deformed single crystals of high-purity iron using positron annihilation: Determination of dislocation densities*. Phys. Rev. **B34** (1986) 823–836.

07 B. Somieski. *Positronenlebensdauerspektroskopie an mechanisch geschädigten Eisenlegierungen*. PhD-thesis. Technische Fakultät der Universität des Saarlandes, 1996.

08 C. Hübner, T.E.M. Staab und R. Krause-Rehberg. *On the Interpretation of Positron-Annihilation Data in Powders and Fine-Grained Materials*. Applied Physics **61** (1995) 203–206.

09 T.E.M. Staab, R. Krause-Rehberg, and B. Kieback, J. Mater. Sci. **34** 3833 (1999)

10 T.E.M. Staab, R. Helm and A. Diegeler. *Sintering Nickel and Iron: Are there Indications for Defect-Activated Sintering.* EURO-PM 2017 (Milan) – Congress Proceedings, EPMA, European Powder Metallurgy Association (EPMA), Shrewsbury, SY1 1LG, United Kingdom

11 T.E.M. Staab, *Defect-Activated Sintering: Really Necessary to Explain High Shrinkage Rates?*, World-PM 2016 Hamburg – Congress Proceedings, EPMA, European Powder Metallurgy Association (EPMA), Shrewsbury, SY1 1LG, United Kingdom

12 I. Gibson, D.W. Rosen, B. Stucker, 2015, Additive Manufacturing Technologies: 3D Printing, Rapid Prototyping, and Direct Digital Manufacturing, Springer, pp. 1–498.

13 A. Zavaliangos, J.M. Missiaen and D. Bouvard. *Anisotropy in Shrinkage During Sintering*. Science of Sintering **38** (1) (2006) 13-25

14 B.X. Peng, J.Y. Jin, Y.S. Liu, Z.H. Zhang, M. Yan, Effects of (Nd, Pr)-Hx addition on the coercivity of Nd-Ce-Y-Fe-B sintered magnet J. Alloys Compd., 772 (2018), pp. 656-662.

15 T.Y. Ma, M. Yan, K.Y. Wu, B. Wu, X.L. Liu, X.J. Wang, Z.Y. Qian, C. Wu, W.X. XiaGrain boundary restructuring of multi-main-phase Nd-Ce-Fe-B sintered magnets with Nd hydrides Acta Mater., 142 (2018), pp. 18-28

16 X. Tang, H. Sepehri,Amin, T. Ohkubo, M. Yano, M. Ito, A. Kato, N. Sakuma, T. Shoji, T. Schrefl, K. HonoCoercivity enhancement of hot-deformed Ce-Fe-B magnets by grain boundary infiltration of Nd-Cu eutectic alloy Acta Mater., 144 (2018), pp. 884-895